Control of Localized Single- and Many-Body Dark States in Waveguide QED

R. Holzinger,[1] R. Gutiérrez-Jáuregui,[2] T. Hönigl-Decrinis,[3,4] G. Kirchmair,[3,4] A. Asenjo-Garcia,[2] and H. Ritsch[1]
[1]*Institute for Theoretical Physics, Innsbruck University, Technikerstrasse 21a, 6020 Innsbruck, Austria*
[2]*Department of Physics, Columbia University, New York, New York 10027, USA*
[3]*Institute for Quantum Optics and Quantum Information, Austrian Academy of Sciences, 6020 Innsbruck, Austria*
[4]*Institute for Experimental Physics, University of Innsbruck, 6020 Innsbruck, Austria*

(Received 27 September 2022; revised 24 October 2022; accepted 22 November 2022; published 14 December 2022; corrected 6 September 2023)

Subradiant states in a finite chain of two-level quantum emitters coupled to a one-dimensional reservoir are a resource for superior photon storage and their controlled release. As one can maximally store one energy quantum per emitter, storing multiple excitations requires delocalized states, which typically exhibit fermionic correlations and antisymmetric wave functions, thus making them hard to access experimentally. Here we identify a new class of quasilocalized dark states with up to half of the qubits excited, which only appear for lattice constants of an integer multiple of the wavelength. These states allow for a high-fidelity preparation and minimally invasive readout in state-of-the-art setups. In particular, we suggest an experimental implementation using a coplanar waveguide coupled to superconducting transmon qubits on a chip. With minimal free space and intrinsic losses, virtually perfect dark states can be achieved for a low number of qubits featuring fast preparation and precise manipulation.

DOI: 10.1103/PhysRevLett.129.253601

Introduction.—Collective excitation states of ensembles of quantum emitters possess several surprising and long-sought physical properties. Typically, excitations are delocalized and lost dissipatively to the environment at rates that vary over many orders of magnitude. Of particular interest are states with long lifetimes. These dark—or subradiant—states can be used to implement extremely efficient quantum memories [1,2], lossless transport of excitations [3,4], photon-photon gates [5], future generations of atomic lattice clocks [6,7], and improve quantum sensing. Recently, applications toward building superior single photon antennas [8] or nanoscopic coherent or nonclassical light sources based on dark resonances have been proposed [9].

In most cases, studies and experiments on subradiance focus on manipulating a single excitation only; i.e., they limit their scope to the lowest Dicke manifold [9–21]. Many-body multiple excitation subradiant states have attracted some interest only recently, but in general the preparation and manipulation of such states remains challenging as they are typically very delocalized. One option is to use more complex atomic emitters with several internal excited states. This allows us to store several photons in a dark subspace, but they are tied to multipartite entanglement, which is fragile in general [22–27]. For a chain of qubits coupled to a waveguide, dark states within the two-excitation manifold have been classified into fermionic, dimerized, or edge states among others [28–42]. Experimental preparation and control of such states remains challenging and only quite recently the two-excitation manifold was probed experimentally with superconducting transmon qubits [43].

In this Letter, we theoretically predict a new type of many-body dark states for arrays of qubits coupled to a 1D bath. These states emerge when the lattice constant is an integer of the guided mode wavelength and are distinguished by strongly localized excitations. The states are built from antisymmetric superpositions of symmetric states, whose decay into the bath is forbidden due to destructive interference [44]. For instance, we find that a large fraction $2(N-3)/(N-2)$ of two excitations stored in an N qubit array settles in just two qubits, while a small fraction spreads along the remaining qubits to inhibit decay [see Fig. 1(c)]. We show below an analytical description for these states and characterize their spatial correlations. We study spectral signatures of photon transport in the presence of these states. From these findings, we propose a realistic protocol to store and release microwave photons in a controlled fashion. Our Letter should lead to multiple opportunities within atomic physics and quantum optics, such as multiphoton memories for quantum repeaters, and unlock rich phenomena in ordered systems of long-range interacting quantum emitters, both in the linear and quantum many-body regimes. We also note that the high-fidelity preparation protocol presented here may inspire experimental confirmation and further the understanding of many-body subradiant states.

Model.—Consider an array of N qubits resonantly coupled to the modes of a waveguide as illustrated in Fig. 1. Each qubit has two internal states $|e_m\rangle$ and $|g_m\rangle$ separated by a transition frequency ω_0 and is characterized by its position x_m. The waveguide mediates the qubit-qubit interactions and acts as a source of dissipation. With the

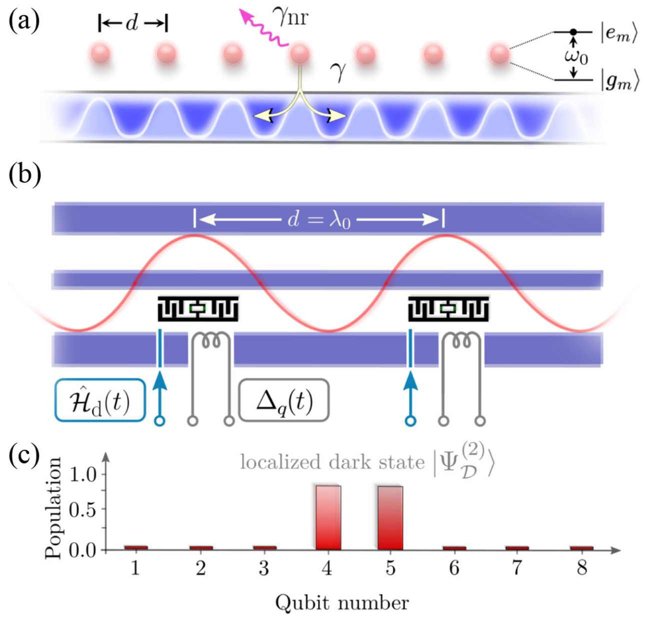

FIG. 1. (a) Schematics of a regular chain of qubits coupled to a 1D waveguide with photon-mediated interactions determined by the single-qubit decay rates γ. For qubits separated by integer multiples of the wavelength λ_0, a degenerate family of nonradiative dark states forms, which are only subject to very small free-space decay and nonradiative losses $\gamma_{\rm nr}$. (b) Waveguide QED realization with superconducting circuits: transmons (in black) are coupled to a coplanar waveguide (in blue). The individual qubit frequencies and thus effectively their distance d can be tuned *in situ* via flux-bias lines. For the preparation and readout of dark states, local driving pulses $\hat{\mathcal{H}}_d(t)$ and local detuning control $\Delta_q(t)$ are applied via separate control lines. (c) Distribution of the excited state population for $N = 8$ qubits for a localized two-excitation dark state $|\Psi_{\mathcal{D}}^{(2)}\rangle$ as described by Eq. (7). Two qubits store a large fraction $2(N-3)/(N-2)$ of the excitation energy.

inclusion of spontaneous emission into the waveguide and assuming that ω_0 is well below the cutoff frequency of the waveguide, the master equation for the density operator of the array $\hat{\rho}$ reads [44,45] $\dot{\hat{\rho}} = -i(\hat{\mathcal{H}}_{\rm eff}\hat{\rho} - \hat{\rho}\hat{\mathcal{H}}_{\rm eff}^\dagger) + \sum_{m,n}\gamma_{m,n}\hat{\sigma}_m\hat{\rho}\hat{\sigma}_n^\dagger$, where $\hat{\mathcal{H}}_{\rm eff}$ is the collective Hamiltonian ($\hbar = 1$),

$$\hat{\mathcal{H}}_{\rm eff} = \sum_{m,n=1}^{N}\left(J_{m,n} - i\frac{\gamma_{m,n}}{2}\right)\hat{\sigma}_m^\dagger\hat{\sigma}_n, \tag{1}$$

composed of lowering operators $\hat{\sigma}_m = |g_m\rangle\langle e_m|$ and interaction terms $J_{m,n} = (\gamma/2)\sin k_0|x_m - x_n|$ and $\gamma_{m,n} = \gamma\cos k_0|x_m - x_n|$. The interaction rate is given by the individual decay rate γ while the qubit separation by $k_0 = \omega_0/c$, the wave vector of the guided mode on resonance with the qubits. For qubit separation $d = n\lambda_0$ with $n \in \mathbb{N}^+$, the coherent exchange rates $J_{m,n}$ are zero and there is only collective dissipation $\gamma_{m,n}$.

We are interested in localized dark states $|\Psi_{\mathcal{D}}^{(M)}\rangle$ storing M excitations. To construct such states, we divide the chain into two parts of M and $N-M$ qubits, respectively. The precise position of the qubits is not relevant for this division, and without losing generality we define the collective operators $\mathcal{S}_1 = \sum_{j=1}^{M}\hat{\sigma}_j/\sqrt{M}$ and $\mathcal{S}_2 = \sum_{j=M+1}^{N}\hat{\sigma}_j/\sqrt{N-M}$ to act over each part. The effective Hamiltonian for $d = n\lambda_0$ within this division reads:

$$\hat{\mathcal{H}}_{\rm eff} = -\frac{iM\gamma}{2}\mathcal{S}_1^\dagger\mathcal{S}_1 - \frac{i(N-M)\gamma}{2}\mathcal{S}_2^\dagger\mathcal{S}_2 - i\Gamma(\mathcal{S}_1^\dagger\mathcal{S}_2 + \mathcal{S}_2^\dagger\mathcal{S}_1). \tag{2}$$

The last term shows that the symmetric superpositions of the two parts are dissipatively coupled by the enhanced rate $2\Gamma = \sqrt{M(N-M)}\gamma$. A similar division can be done for odd multiples of $\lambda_0/2$ separations with the symmetric operators now replaced with antisymmetric operators, having alternate signs between consecutive qubits.

The division is a formal one, but our results can be generalized to nonidentical couplings as shown in the Supplemental Material (SM) [46]. In particular, if we assume that the first qubits decay with a rate γ_1 while the remaining decay with γ_2, the localization is enhanced. That is, a higher fraction of the excited state population is concentrated in the first qubits. The effects of impurities as nonradiative energy loss $\gamma_{\rm nr}$ and dephasing γ_ϕ are also explored in the SM.

Single excitation.—Qubits decay into the waveguide via collective channels determined by the eigenstates of Eq. (1). The decay rates depend on qubit number N and lattice spacing d, as shown in Fig. 2(a) for the slowest decay rate of a single excitation. While in general this rate is suppressed with increasing qubit number—following a N^{-3} scaling [29]—this is not the case for spacing $k_0 d = n\pi$. In the so-called "mirror configuration" (with $d = n\lambda_0$), there is only one bright state, $|\Psi_{\mathcal{S}}^{(1)}\rangle = \sum_j^N\hat{\sigma}_j^\dagger|G\rangle/\sqrt{N}$, where $|G\rangle = |g\rangle^{\otimes N}$, and $(N-1)$ perfectly dark states of exactly zero decay rate. Leveraging the degeneracy of the dark manifold, one can build highly localized dark states. Consider the state

$$|\Psi_{\mathcal{D}}^{(1)}\rangle = \frac{1}{\sqrt{N}}(\sqrt{N-1}\hat{\sigma}_1^\dagger - \mathcal{S}_2^\dagger)|G\rangle, \tag{3}$$

composed of the normalized sum of $|\Psi_m\rangle = 1/\sqrt{2}(\hat{\sigma}_1^\dagger - \hat{\sigma}_m^\dagger)|G\rangle$ states, which span the $N-1$ dark subspace. The operator $\mathcal{S}_2$ is defined above the system Hamiltonian in Eq. (2). The dark state displays the unique feature that a large fraction $\langle\hat{\sigma}_1^\dagger\hat{\sigma}_1\rangle = 1 - 1/N$ of the excited state population is concentrated in the first qubit. By increasing the system size, the excitation is mostly stored in the first qubit while being protected from decay by a vanishing amount spread in the remaining qubits. The absence of coherent exchange interaction is crucial in so far as it would

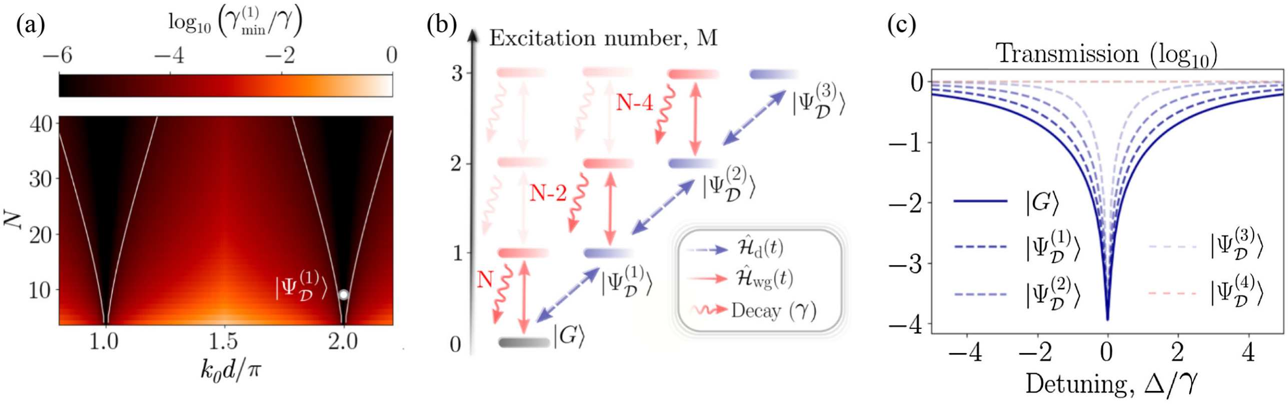

FIG. 2. (a) Minimal decay rate $\gamma^{(1)}_{\min}$ within the single-excitation manifold as a function of qubit number and separation d for lossless qubits with $\gamma_{\rm nr}=0$. Continuous white lines enclose regions of strong collective subradiance, where $\gamma^{(1)}_{\min}/\gamma \le 10^{-5}$. The example of Eq. (3) is indicated with a white dot for $N=8$ qubits. (b) Assuming M qubits are driven individually, we show the energy level diagram indicating the route toward dark state preparation and probing with coupling to $|\Psi^{(M)}_{\mathcal{D}}\rangle$ facilitated by a coherent drive $\hat{\mathcal{H}}_d(t)$. Once $|\Psi^{(M)}_{\mathcal{D}}\rangle$ is prepared a second field sent through the waveguide, as described by $\hat{\mathcal{H}}_{\rm wg}(t)$ in Eq. (6), transfers the state outside the dark manifold, from where it decays with rate $(N-2M)\gamma$. (c) Weak field waveguide transmission as a function of probe frequency tuned across the single-qubit resonance frequency ω_0 for an eight-qubit chain in the ground state (solid line) and the single- to four-excitation dark states (dashed lines). The blockade window decreases from the linewidth $N\gamma$ of the symmetric single-excitation state towards $(N-2M)\gamma$ for the M-excitation dark state and disappears for the four-excitation dark state showing complete transmission.

introduce unwanted couplings between bright and dark states.

Dark state preparation and probing.—The choice to store an excitation in the first qubit is not unique and any other qubit is equally valid [46]. The dark state $|\Psi^{(1)}_{\mathcal{D}}\rangle$, however, can be efficiently prepared by introducing an external coherent drive on resonance with qubits and localized on the first qubit. This pulsed drive couples to the chain via $\hat{\mathcal{H}}_d(t)=\Omega_d(t)(\hat{\sigma}_1^\dagger+\hat{\sigma}_1)$, where $\Omega_d(t)$ is a time-dependent Rabi frequency. It connects the ground state to both bright and dark states with asymmetrical coupling strengths,

$$\langle\Psi^{(1)}_{\mathcal{S}}|\hat{\mathcal{H}}_d(t)|G\rangle=\Omega_d(t)\sqrt{1/N}, \tag{4}$$

$$\langle\Psi^{(1)}_{\mathcal{D}}|\hat{\mathcal{H}}_d(t)|G\rangle=\Omega_d(t)\sqrt{1-1/N}, \tag{5}$$

thus coupling to the dark state with high fidelity in the $N\gg 1$ limit. The drive not only prepares single-excitation dark states but also connects dark states along the excitation ladder through paths illustrated in Fig. 2(b). These paths continue until half of the qubits are excited and there are no more dark states [36].

To probe the dark states we use a second, weak driving field $[\Omega_{\rm wg}(t)/\gamma\ll 1]$. The field propagates along the waveguide and couples to the qubits through

$$\hat{\mathcal{H}}_{\rm wg}(t)=\sum_{j=1}^{N}\left(\Delta_{\rm wg}\hat{\sigma}_j^\dagger\hat{\sigma}_j+\Omega_{\rm wg}(t)(\hat{\sigma}_j^\dagger+\hat{\sigma}_j)\right). \tag{6}$$

Note that there is no phase pickup between the qubits due to the $n\lambda_0$ separation. This probe connects dark and bright states through paths shown in Fig. 2(b). It then opens a window into the dark states by measuring the field $\hat{E}=\hat{E}_{\rm in}+i\sqrt{\gamma/2}\sum_j\hat{\sigma}_j$ composed from the superposition of probe and fields scattered into the waveguide. Figure 2(c) shows the transmission $\langle\hat{E}^\dagger\hat{E}\rangle/\langle\hat{E}^\dagger_{\rm in}\hat{E}_{\rm in}\rangle$ for different initial states. An eight-qubit chain is probed by a rectangular waveguide pulse of duration $t\gamma=50$ during which the transmitted field is recorded using the master equation accounting for multiple excitations [10]. We begin with N qubits in the ground state where the transmission linewidth is $N\gamma$, corresponding to the symmetric state $|\Psi^{(1)}_{\mathcal{S}}\rangle$ excited by the probe. For the qubits prepared in the Mth excitation dark state, the transmission linewidth is reduced to $(N-2M)\gamma$ [46]. For a single excitation, with $N\ge 3$, the probe excites $\hat{\mathcal{H}}_{\rm wg}(t)|\Psi^{(1)}_{\mathcal{D}}\rangle\propto|\Psi^{(2)}\rangle$, with $|\Psi^{(2)}\rangle\propto[(N-2)\sigma_1^\dagger-\sqrt{N-1}\mathcal{S}_2^\dagger]\mathcal{S}_2^\dagger|G\rangle$. For $M=N/2$ the waveguide drive is orthogonal to the dark state and therefore renders the system completely transparent. In this way the two-excitation manifold is utilized to escape the decoherence-free subspace and probe the preparation of the dark state [43].

Note that we assume the ideal case without imperfections and positional disorder, which would lead to a finite lifetime of the dark state and a higher overall transmission, treated in the SM [46].

Multiple excitations.—The localized dark states for multiple excitations are written explicitly in the SM [46]. For simplicity, we focus on the two-excitation subspace of

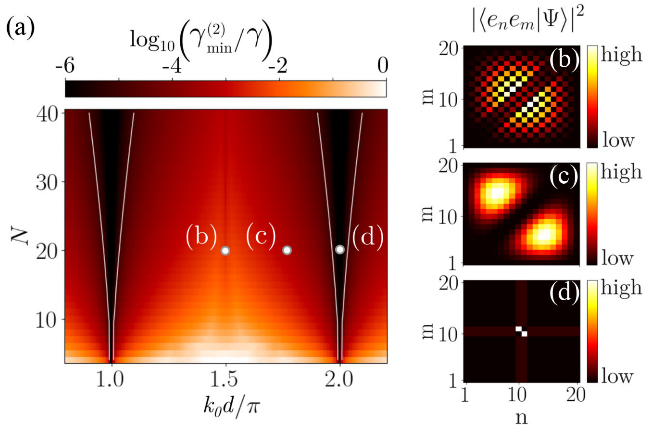

FIG. 3. (a) Minimal decay rate $\gamma^{(2)}_{\min}$ within the second excitation manifold as a function of chain size N and qubit separation d. The continuous white lines enclose the regions where $\gamma^{(2)}_{\min}/\gamma \leq 10^{-5}$. The subradiant states generally exhibit nontrivial spatial correlations $|\langle e_n e_m|\Psi\rangle|^2$, which renders them challenging to access. For $k_0 d = (2n+1)\pi/2$ with $n \in \mathbb{N}$, a checkerboard pattern emerges in (b) whereas in (c) a typical fermionic occupation is shown, which is shared by most subradiant states. In (d) the dark state $|\Psi^{(2)}_{\mathcal{D}}\rangle$, of Eq. (7), is shown for $k_0 d = 2n\pi$ with two excitations localized in the center of the array.

Eq. (2), where the Hilbert space is spanned by states $|e_n e_m\rangle = \hat{\sigma}^\dagger_n \hat{\sigma}^\dagger_m |G\rangle$. In general, the most superradiant two-excitation state can be written as $|\Psi^{(2)}_{\mathcal{S}}\rangle \propto \sum_{j<k} \hat{\sigma}^\dagger_j \hat{\sigma}^\dagger_k |G\rangle$ and decay with a rate $2(N-1)\gamma$. By contrast, for $k_0 d = n\pi$, a completely dark state is

$$|\Psi^{(2)}_{\mathcal{D}}\rangle = \frac{\sqrt{N-3}}{\sqrt{N-1}}\left((\mathcal{S}^\dagger_1)^2 - \frac{\sqrt{2}\mathcal{S}^\dagger_1\mathcal{S}^\dagger_2}{\sqrt{N-2}} + \frac{(\mathcal{S}^\dagger_2)^2}{N-3}\right)|G\rangle, \qquad (7)$$

where a fraction $2(N-3)/(N-2)$ of the excitations is stored in the first two qubits with $\mathcal{S}_{1,2}$ defined above Eq. (2).

Subradiant states for two excitations are illustrated in Fig. 3. Figure 3(a) shows the minimal decay rate $\gamma^{(2)}_{\min}$ as a function of qubit number N and relative distance d. The decay rate changes with lattice constant and signals different types of dark states with qualitatively different spatial correlations $|\langle e_n e_m|\Psi\rangle|^2$, as shown in Figs. 3(b)–3(d). For $k_0 d = (2n+1)\pi/2$ with $n \in \mathbb{N}$, correlations display a checkerboard-type pattern [29] due to the fact that coherent nearest-neighbor and dissipative next-nearest-neighbor interactions in Eq. (1) are zero. Figure 3(c) shows a typical state, described by a fermionic ansatz, where two-excitation states are composed of single-excitation subradiant states, as commonly found for multiple excitations [1,28]. For a large number of qubits, $N \gtrsim 50$ and $k_0 d = (6n-1)\pi/6$, another extremely subradiant two-excitation state emerges with dimerized spatial correlations and a decay rate lower than any fermionic-type state [31]. These extended states are to be compared with Fig. 3(d), where the dark state $|\Psi^{(2)}_{\mathcal{D}}\rangle$ of Eq. (7) with $k_0 d = 2\pi n$ is shown for a 20-qubit chain. The spatial correlations of the dark state lead to easily accessible preparation as opposed to most other subradiant states with nontrivial spatial correlations. For instance, a (local) coherent drive with Rabi frequency $\Omega_d(t)$ exciting two of the qubits drives the dark state with strength $\Omega_d(t)\sqrt{N-3}/\sqrt{N-1}$ and subsequently a waveguide drive can be used to probe the preparation of the dark state; see also Fig. 2(b).

Two-photon storage and release.—Building on the above results we establish a simple protocol for storing and releasing two excitations into a waveguide. The protocol starts with N qubits in the ground state that are driven into the dark state $|\Psi^{(2)}_{\mathcal{D}}\rangle$ by a coherent pulse on the first two qubits. The two excitations remain stored for a time τ after which the last $N-2$ qubits are detuned by $\Delta_q \gtrsim (N-2)\gamma$ to transfer most of the two excitations into the product state $|e_1 e_2\rangle$. This is illustrated in Fig. 4 for a

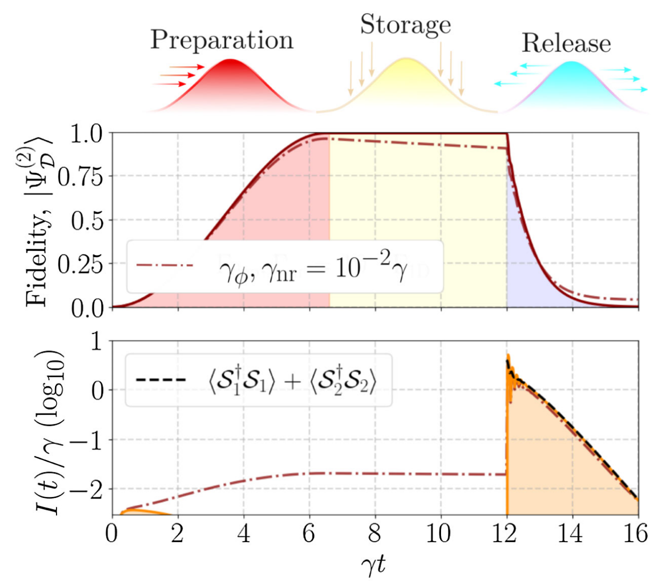

FIG. 4. Protocol to prepare, store, and release two excitations using a chain of 16 qubits separated a distance $d = \lambda_0$. (a) A π pulse drives the first two qubits into the dark state $|\Psi^{(2)}_{\mathcal{D}}\rangle$ where excitations are stored until $\gamma t = 12$, when they are released via a superradiant channel created by quickly detuning the last $N-2$ qubits by $\Delta_q = 50\gamma$. (b) Fidelity $F = \langle\Psi^{(2)}_{\mathcal{D}}|\rho|\Psi^{(2)}_{\mathcal{D}}\rangle$ to prepare the dark state for an ideal case (solid line) compared to a case with dephasing and nonradiative damping $\gamma_{\rm dep}, \gamma_{\rm nr} = 10^{-2}\gamma$ (dash-dotted line). (c) The field radiated into the waveguide displays a sharp peak in intensity $I(t) = \langle\hat{E}^\dagger\hat{E}\rangle(t)$ after release and negligible values during preparation and storage. A beating in intensity appears as the excitation oscillates between initial and final qubits during release [see $\hat{\mathcal{S}}_{1,2}$ in Eq. (2)]. Emission with (dash-dotted line) and without interference term $2\mathrm{Re}\langle\mathcal{S}^\dagger_1\mathcal{S}_2\rangle$ (black dashed line). Here, the π pulse has a Gaussian temporal profile of duration 8γ at FWHM and reaches a peak Rabi frequency 0.25γ at $t_0 = 3\gamma^{-1}$.

16-qubit chain with and without imperfections. The coherent drive $\hat{\mathcal{H}}_d(t) = \Omega_d(t)(\hat{\sigma}_1^\dagger + \hat{\sigma}_2^\dagger + \mathrm{H.c.})$ prepares the state $|\Psi_{\mathcal{D}}^{(2)}\rangle$. Then, at $\gamma t = 12$, the last 14 qubits are detuned by $\Delta_q = 50\gamma$ from the resonance frequency ω_0 to initiate the decay of excitations. The radiated intensity $I(t) = \langle \hat{E}^\dagger \hat{E}\rangle(t)$, equivalently expressed as $\langle \mathcal{S}_1^\dagger \mathcal{S}_1\rangle + \langle \mathcal{S}_2^\dagger \mathcal{S}_2\rangle + 2\mathrm{Re}\langle \mathcal{S}_1^\dagger \mathcal{S}_2\rangle$, is negligible until a sharp pulse of emission appears after the detuning is turned on.

Superconducting circuit implementation.—Because of near-perfect mode matching, superconducting qubits in a 1D transmission line [10,55–57] are an ideal platform for realizing these ideas. Here, we focus on the implementation with transmon qubits capacitively coupled to a common coplanar waveguide as shown schematically in Fig. 1(c). Similar to Ref. [58], the distance d between the qubits on chip is fixed, but changing the frequency at which the transmon qubits emit effectively changes their separation. This ensures that we can satisfy $d \sim \lambda_0$, as well as tune qubits on and off resonance via on-chip flux lines. Weakly coupled control lines realize the drive $\hat{\mathcal{H}}_d(t)$ and allow us to selectively excite the single qubits respectivley *in situ*, and thus prepare dark states [43]. Nonradiative decay rates γ_{nr} and dephasing rates γ_ϕ for superconducting qubits are usually multiple orders of magnitude smaller than typical couplings to the waveguide γ; see the SM [46]. The achievable parameters are easily sufficient to realize the protocol demonstrated in Fig. 4 with ~99% fidelity for the dark state preparation.

Conclusions.—Motivated by state-of-the-art implementations of waveguide-coupled superconducting qubits, we introduced and studied a theoretical model of the properties and excitation pathways of multiexcitation dark states. Because of the symmetry and (practically infinite-range) all to all coupling, such system possesses almost degenerate manifolds of multiexcitation states radiatively decoupled from the waveguide if the qubits are positioned at wavelength distance. These states allow us to absorb and store multiple photons simultaneously [46], while localizing the majority of the excitation energy in just a handful of qubits. This contrasts with typical free-space subradiant states, where each excitation is maximally delocalized. Their localized nature facilitates the preparation of these states via local addressing of individual qubits, which is currently available in state-of-the-art implementations. The system and the proposed protocol also allow for controlled storage and release of multiple photons into the waveguide, pointing toward possible applications for nonclassical multiphoton sources or a tailored memory for a quantum repeater. As the projected numbers for experimental realizations seem favorable, we expect to inspire efforts in various quantum simulation platforms including superconducting circuits or Rydberg arrays [7,59]. Similarly, optical waveguide systems [14] and atoms, which are tweezer trapped in optical resonators [60], can be envisaged as an alternative setup.

R. H. and H. R. acknowledge funding from the Austrian Science Fund (FWF) doctoral college DK-ALM W1259-N27 and the FET OPEN Network Cryst3 funded by the European Union (EU) via Horizon 2020. T. H-D. acknowledges financial support from the Lise Meitner program of the Austrian Science Fund (FWF), Project No. M3347. A. A.-G. gratefully acknowledges support from the U.S. Air Force Office of Scientific Research through their Young Investigator Prize (Grant No. 21RT0751), the National Science Foundation through their CAREER Award (No. 2047380), the A. P. Sloan foundation, and the David and Lucile Packard foundation. G. K. acknowledges funding by the European Research Council (ERC) under the European Union's Horizon 2020 research and innovation program (714235).

[1] A. Asenjo-Garcia, M. Moreno-Cardoner, A. Albrecht, H. J. Kimble, and D. E. Chang, Phys. Rev. X **7**, 031024 (2017).
[2] M. Moreno-Cardoner, D. Plankensteiner, L. Ostermann, D. E. Chang, and H. Ritsch, Phys. Rev. A **100**, 023806 (2019).
[3] S. J. Masson and A. Asenjo-Garcia, Phys. Rev. Res. **2**, 043213 (2020).
[4] R. Gutiérrez-Jáuregui and A. Asenjo-Garcia, Phys. Rev. A **105**, 043703 (2022).
[5] M. Moreno-Cardoner, D. Goncalves, and D. E. Chang, Phys. Rev. Lett. **127**, 263602 (2021).
[6] I. S. Madjarov, A. Cooper, A. L. Shaw, J. P. Covey, V. Schkolnik, T. H. Yoon, J. R. Williams, and M. Endres, Phys. Rev. X **9**, 041052 (2019).
[7] M. A. Norcia, A. W. Young, W. J. Eckner, E. Oelker, J. Ye, and A. M. Kaufman, Science **366**, 93 (2019).
[8] M. Moreno-Cardoner, R. Holzinger, and H. Ritsch, Opt. Express **30**, 10779 (2022).
[9] R. Holzinger, M. Moreno-Cardoner, and H. Ritsch, Appl. Phys. Lett. **119**, 024002 (2021).
[10] M. Mirhosseini, E. Kim, X. Zhang, A. Sipahigil, P. B. Dieterle, A. J. Keller, A. Asenjo-Garcia, D. E. Chang, and O. Painter, Nature (London) **569**, 692 (2019).
[11] M. T. Manzoni, M. Moreno-Cardoner, A. Asenjo-Garcia, J. V. Porto, A. V. Gorshkov, and D. E. Chang, New J. Phys. **20**, 083048 (2018).
[12] K. E. Ballantine and J. Ruostekoski, PRX Quantum **2**, 040362 (2021).
[13] D. F. Kornovan, N. V. Corzo, J. Laurat, and A. S. Sheremet, Phys. Rev. A **100**, 063832 (2019).
[14] N. V. Corzo, J. Raskop, A. Chandra, A. S. Sheremet, B. Gouraud, and J. Laurat, Nature (London) **566**, 359 (2019).
[15] B. Olmos, G. Buonaiuto, P. Schneeweiss, and I. Lesanovsky, Phys. Rev. A **102**, 043711 (2020).
[16] T. Orell, M. Zanner, M. L. Juan, A. Sharafiev, R. Albert, S. Oleschko, G. Kirchmair, and M. Silveri, Phys. Rev. A **105**, 063701 (2022).
[17] X.-L. Chu, V. Angelopoulou, P. Lodahl, and N. Rotenberg, Phys. Rev. A **106**, 053702 (2022).
[18] Y. He, L. Ji, Y. Wang, L. Qiu, J. Zhao, Y. Ma, X. Huang, S. Wu, and D. E. Chang, Phys. Rev. Lett. **125**, 213602 (2020).

[19] O. Rubies-Bigorda, V. Walther, T. L. Patti, and S. F. Yelin, Phys. Rev. Res. **4**, 013110 (2022).
[20] R. J. Bettles, S. A. Gardiner, and C. S. Adams, Phys. Rev. A **94**, 043844 (2016).
[21] V. Paulisch, H. J. Kimble, and A. González-Tudela, New J. Phys. **18**, 043041 (2016).
[22] A. Asenjo-Garcia, H. J. Kimble, and D. E. Chang, Proc. Natl. Acad. Sci. U.S.A. **116**, 25503 (2019).
[23] A. González-Tudela, V. Paulisch, H. J. Kimble, and J. I. Cirac, Phys. Rev. Lett. **118**, 213601 (2017).
[24] R. Holzinger, L. Ostermann, and H. Ritsch, Europhys. Lett. **128**, 44001 (2020).
[25] O. Rubies-Bigorda, S. Ostermann, and S. F. Yelin, arXiv: 2209.00034.
[26] Q.-M. Chen, Y.-x. Liu, L. Sun, and R.-B. Wu, Phys. Rev. A **98**, 042328 (2018).
[27] A. González-Tudela, V. Paulisch, D. E. Chang, H. J. Kimble, and J. I. Cirac, Phys. Rev. Lett. **115**, 163603 (2015).
[28] Y.-X. Zhang and K. Mølmer, Phys. Rev. Lett. **122**, 203605 (2019).
[29] A. Albrecht, L. Henriet, A. Asenjo-Garcia, P. B. Dieterle, O. Painter, and D. E. Chang, New J. Phys. **21**, 025003 (2019).
[30] L. Henriet, J. S. Douglas, D. E. Chang, and A. Albrecht, Phys. Rev. A **99**, 023802 (2019).
[31] Y.-X. Zhang, C. Yu, and K. Mølmer, Phys. Rev. Res. **2**, 013173 (2020).
[32] B. Bakkensen, Y.-X. Zhang, J. Bjerlin, and A. S. Sørensen, arXiv:2110.06093.
[33] Y.-L. L. Fang, H. Zheng, and H. U. Baranger, Eur. Phys. J. Quantum Technol. **1**, 3 (2014).
[34] J. Zhong, N. A. Olekhno, Y. Ke, A. V. Poshakinskiy, C. Lee, Y. S. Kivshar, and A. N. Poddubny, Phys. Rev. Lett. **124**, 093604 (2020).
[35] A. S. Sheremet, M. I. Petrov, I. V. Iorsh, A. V. Poshakinskiy, and A. N. Poddubny, arXiv:2103.06824.
[36] A. V. Poshakinskiy and A. N. Poddubny, Phys. Rev. Lett. **127**, 173601 (2021).
[37] A. V. Poshakinskiy, J. Zhong, Y. Ke, N. A. Olekhno, C. Lee, Y. S. Kivshar, and A. N. Poddubny, npj Quantum Inf. **7**, 34 (2021).
[38] S. D. Jenkins, J. Ruostekoski, N. Papasimakis, S. Savo, and N. I. Zheludev, Phys. Rev. Lett. **119**, 053901 (2017).
[39] Y. Ke, A. V. Poshakinskiy, C. Lee, Y. S. Kivshar, and A. N. Poddubny, Phys. Rev. Lett. **123**, 253601 (2019).
[40] S. J. Masson, I. Ferrier-Barbut, L. A. Orozco, A. Browaeys, and A. Asenjo-Garcia, Phys. Rev. Lett. **125**, 263601 (2020).
[41] N. Fayard, L. Henriet, A. Asenjo-Garcia, and D. E. Chang, Phys. Rev. Res. **3**, 033233 (2021).
[42] J. Zhong and A. N. Poddubny, Phys. Rev. A **103**, 023720 (2021).
[43] M. Zanner, T. Orell, C. M. F. Schneider, R. Albert, S. Oleschko, M. L. Juan, M. Silveri, and G. Kirchmair, Nat. Phys. **18**, 538 (2022).
[44] K. Lalumière, B. C. Sanders, A. F. van Loo, A. Fedorov, A. Wallraff, and A. Blais, Phys. Rev. A **88**, 043806 (2013).
[45] D. E. Chang, L. Jiang, A. V. Gorshkov, and H. J. Kimble, New J. Phys. **14**, 063003 (2012).
[46] See Supplemental Material at http://link.aps.org/supplemental/10.1103/PhysRevLett.129.253601, for a general description of the M-excitation dark state, the dynamics between bright and dark state manifolds, the effect of positional disorder and imperfections, and the multilevel nature of the transmon, which includes Refs. [47–54].
[47] M. Gross and S. Haroche, Phys. Rep. **93**, 301 (1982).
[48] M. J. Collett and C. W. Gardiner, Phys. Rev. A **30**, 1386 (1984).
[49] H. J. Carmichael, *Statistical Methods in Quantum Optics 1* (Springer-Verlag, Berlin, 1999), Chap. 2.
[50] J. Larson and T. Mavrogordatos, *The Jaynes–Cummings Model and Its Descendants* (IOP Publishing, Bristol, 2021).
[51] A. Blais, A. L. Grimsmo, S. M. Girvin, and A. Wallraff, Rev. Mod. Phys. **93**, 025005 (2021).
[52] R. H. Lehmberg, Phys. Rev. A **2**, 883 (1970).
[53] G. S. Agarwal, Phys. Rev. A **7**, 1195 (1973).
[54] R. Holzinger, D. Plankensteiner, L. Ostermann, and H. Ritsch, Phys. Rev. Lett. **124**, 253603 (2020).
[55] O. Astafiev, A. M. Zagoskin, A. A. Abdumalikov, Y. A. Pashkin, T. Yamamoto, K. Inomata, Y. Nakamura, and J. S. Tsai, Science **327**, 840 (2010).
[56] T. Hönigl-Decrinis, R. Shaikhaidarov, S. de Graaf, V. N. Antonov, and O. V. Astafiev, Phys. Rev. Appl. **13**, 024066 (2020).
[57] J. D. Brehm, R. Gebauer, A. Stehli, A. N. Poddubny, O. Sander, H. Rotzinger, and A. V. Ustinov, Appl. Phys. Lett. **121**, 204001 (2022).
[58] A. F. van Loo, A. Fedorov, K. Lalumière, B. C. Sanders, A. Blais, and A. Wallraff, Science **342**, 1494 (2013).
[59] E. Kuznetsova, S. T. Rittenhouse, H. R. Sadeghpour, and S. F. Yelin, Phys. Rev. A **94**, 032325 (2016).
[60] N. Sauerwein, F. Orsi, P. Uhrich, S. Bandyopadhyay, F. Mattiotti, T. Cantat-Moltrecht, G. Pupillo, P. Hauke, and J.-P. Brantut, arXiv:2208.09421.

Correction: The affiliations for the third and fourth authors were incomplete and have been rectified, and a fourth affiliation has been added.